A Comparison of Rotation- and Blob-Based System Models for 3-D SPECT with Depth-Dependent Detector Response

Anastasia Yendiki and Jeffrey A. Fessler
Department of Electrical Engineering and Computer Science
University of Michigan, Ann Arbor, MI, USA
E-mail: nastazia@eecs.umich.edu

I. Introduction

Statistical reconstruction is now widely used in computed tomography, as it is known to produce higher image quality than analytical methods such as Filtered Back-Projection (FBP). However, this improved quality is achieved at the cost of increased computation time. A key component of the accuracy-computation trade-off in the iterative algorithms used for statistical image reconstruction is that typically one projection and one backprojection operation have to be performed at each iteration of the algorithm. The implementation of these operations requires a model for the imaging system at hand. In general, a more detailed model will result in higher image quality but also in higher computational load, which can become especially cumbersome in 3-D problems.

In this paper we focus on system models for 3-D Single-Photon Emission Computed Tomography (SPECT) that compensate for non-uniform attenuation as well as the depth-dependent response inherent in SPECT systems. More specifically, we consider here rotation- and blob-based implementations. Several rotation-based models have been found to achieve superior accuracy when compared to the simple line-integral model in 2-D reconstruction [1]. Furthermore, models that represent images in terms of spherically symmetric blobs have been applied to 3-D Positron-Emission Tomography (PET) and have been found to possess better noise-resolution properties than models using cubic voxel representations [2]. The blob-based methods are computationally tractable in PET when the "footprint" (2-D projection) of the 3-D blob is precomputed and saved. However, it is not clear if the same holds true for SPECT, where the depth-dependent blur causes these footprints to expand considerably with increasing distance from the detector. Also, for the purpose of SPECT reconstructions, it is of interest to know how these blob-based models compare in terms of noise-resolution properties and speed to the rotation-based models.

We have implemented both types of system model for fully 3-D SPECT and we present preliminary results from reconstructions of simulated phantom data.

II. System models

For both types of system model we have implemented the back-projector as the exact adjoint of the respective projector. Using a simpler back-projector can speed up reconstruction but it does not preserve the convergence properties of the iterative reconstruction algorithm and it introduces artifacts that may accumulate with every iteration [3]. In order to ensure a comparison untarnished of such artifacts, we utilized adjoint pairs.

Both types of system model compensate for nonuniform attenuation. For the sake of speed, the attenuation factors are pre-computed for every volume element (voxel or blob) at every projection angle. Utilizing the central-ray approximation, an attenuation factor is computed by summing over the attenuation map along the perpendicular line from the center of the volume element to the detector.

A. Rotation-based projector

The projector we use performs rotations using the fast and accurate 3-pass separable method described in [4]. This method decomposes the rotation of a 2-D image into three sets of 1-D interpolations. These interpolations are equivalent to applying appropriate non-integer shifts first to each row, then to each column, and then again to each row of the image.

Projectors utilizing the 3-pass method with linear and cubic interpolation have been compared in [1] and the latter outperformed line-integral projector in projection accuracy. However, cubic interpolation introduces negative values in the rotated image, which is unnatural in emission tomography, where image values represent photon counts. Thus, we use linear interpolation hereafter.

The rotation-based 3-D SPECT projector implemented for this comparison compensates for depth-dependent detector response. For every projection angle, it first rotates the input emission volume around its z-axis by applying the 3-pass method to every slice of the volume separately. It then applies to every voxel the appropriate attenuation factor. Subsequently, every image plane that corresponds to a different distance from the detector face is blurred by a 2-D convolution kernel that models the detector response at the corresponding distance. Finally, the voxels are summed along the direction that is perpendicular to the detector to produce a 2-D projection of the emission volume.

B. Blob-based projector

Rotationally symmetric volume elements can provide a basis more natural than cubic voxels for the representation of smooth radioactivity distributions. Moreover, their symmetry makes them appealing for image reconstruction applications since the line integrals through them are independent of projection angle and only depend on the distance of the line of integration from the center of the element [5], [6].

Desired properties of the rotationally symmetric functions are effective band-limitedness (in order to match the band-limitedness of tomographic data) and finite spatial support (in order to facilitate computation). A near-optimal and easy to compute choice is the Kaiser-Bessel blob.

We have implemented a 3-D SPECT projector utilizing Kaiser-Bessel blobs, similar to the one described for PET in [2]. The difference is that the blobs at each different distance from the detector now need to be blurred by the corresponding point-spread function (PSF) of the SPECT detector. By assuming the same detector response throughout a single blob, projecting the blurred blob is equivalent to blurring the projections of the blob. Thus, we can pre-compute and save a set of finely sampled 2-D footprints of the blob, blurred by the detector PSF at each of the distances considered. The attenuation is also assumed to be the same throughout a single blob. The blobs are assumed to be arranged over a uniform 3-D grid. At each projection angle, the position of every blob in the volume is computed. The footprint corresponding to the distance of the blob from the detector is selected, multiplied by the appropriate attenuation factor and the coefficient of the blob and added onto the projection plane at the appropriate position.

The images that are reconstructed using this projector/back-projector pair are blob space representations and thus an extra step of convolution with the blob function is required after reconstruction if the image is to be displayed or compared to images represented in voxel space.

III. Preliminary results

We intend to use larger data sets for our final results but in these preliminary simulations we reconstructed a $64 \times 64 \times 23$ anthropomorphic chest phantom (shown in Figure 1) from projections taken at 60 uniformly spaced angles over a $[0, 2\pi)$ range. The heart, liver, lungs, spine, and surrounding tissue in the phantom have uniform radioactivity densities with ratio 4:3:1:0:2 and uniform attenuation coefficients equal to $0.011, 0.011, 0.002, 0.014$ and 0.011mm^{-1} respectively, values appropriate for the 360KeV photons emitted by I-131.

The pixel size of the system was set to 7.196mm. The depth-dependent PSFs were assumed to be 2-D Gaussians with a Full Width at Half Maximum (FWHM) increasing from 3 to 43mm. These were FWHM values obtained from fitting point-source images acquired on an ultra-high energy collimator. The same set of PSFs were used at all projection angles, as in a circular orbit.

The projections were generated from a high-resolution version of the phantom image using a rotation-based projector and were then downsampled. Images were reconstructed using each system model for 20 iterations of the Ordered Subsets Expectation Maximization (OSEM) algorithm with 10 subsets. Figure 2 shows a slice of the reconstructed images and a profile of this slice through the heart area.

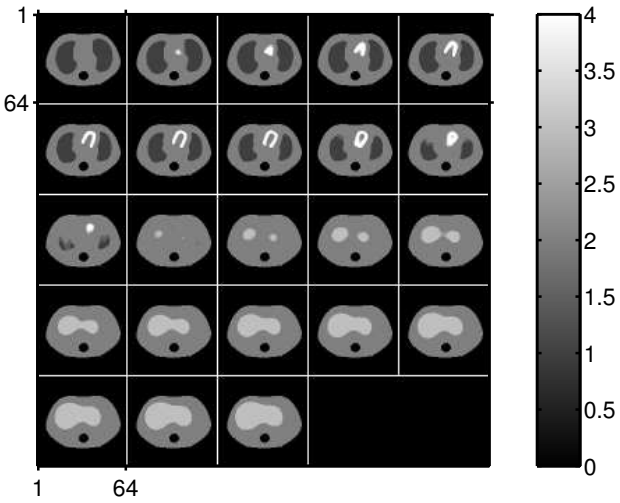

Fig. 1. Anthropomorphic chest phantom

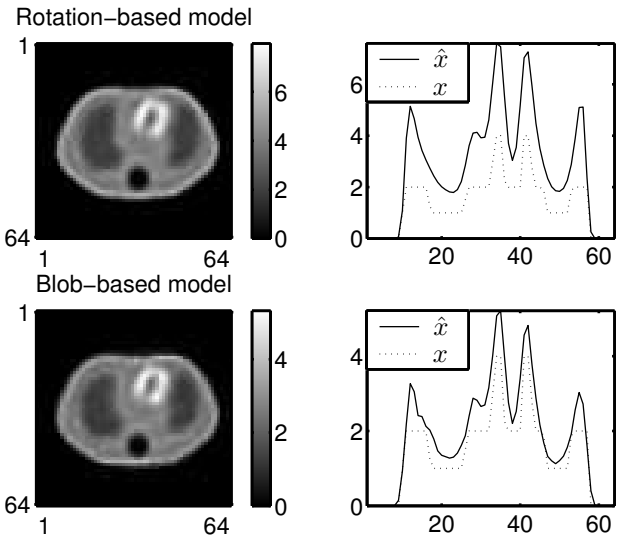

Fig. 2. Reconstruction of noiseless data (The solid line shows the reconstructed image, and the dotted line the true phantom)

Subsequently, we normalized the projection set to a total of 5×10^6 counts. To crudely simulate scatter, we uniformly added to the projection set a number of scattered counts equal to 10% of the total true counts. We used this new projection set to generate Poisson-distributed measurements. Images were reconstructed from the noisy Poisson data using each system model for 30 iterations of the Ordered Subsets Paraboloidal Surrogates (OSPS) algorithm with 10 subsets and regularization parameter $\beta = 0.5$. Figure 3 shows again a slice

of the reconstructed images and a profile of this slice through the heart area.

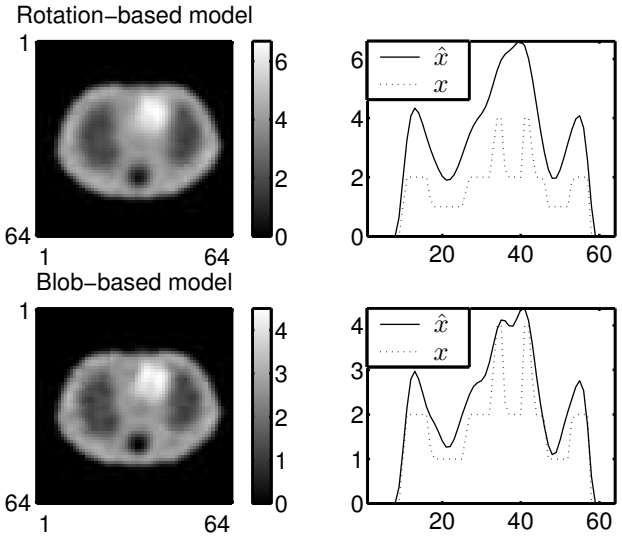

Fig. 3. Reconstruction of noisy data (The solid line shows the reconstructed image, and the dotted line the true phantom)

The images show that the blob-based system significantly reduced bias in both cases. The rotation-based projector has especially high bias around the edges of the phantom, where interpolation is most problematic. The profiles also indicate that there may be a difference in the convergence rate of the algorithms with each system model. We intend to investigate the variance-bias properties of the two systems in greater depth and provide variance-bias plots. The blob-based reconstruction in Figure 3 seems to suffer from a grid-like artifact, that is probably due to coarse sampling of the blob footprint. We are also investigating the effect that the footprint sample spacing, as well as other parameters associated with the Kaiser-Bessel blob, have on the reconstruction.

The CPU time required for calculating a full projection set of the image with the parameters described above on a dual-processor 800MHz Pentium III with 256Kb cache and 1Gb RAM is roughly 4.8s for the rotationbased model and 16.8s for the blob-based model. However our blob projector is still work in progress and does not take advantage of all the possible pre-computations. Currently it pre-computes and saves the attenuation coefficients for all blob grid positions at all angles, as well as the nearest grid position for any blob in a slice at any rotation angle and the limits of the detector area shadowed by any blob at any rotation angle.

Furthermore, the rotation-based model is especially fast in this case because we are assuming a system with perfectly symmetric, separable PSFs and thus the blurring of each image plane can be performed very fast with symmetric 1-D convolutions. If we wanted to model collimator properties in greater detail with non-symetric PSFs we would probably resort to 2-D FFTs and applying a 2-D FFT to every plane in the image at every angle would significantly increase the computation load. The blob-based model would not be affected by this, since the PSFs are only applied to the basic blob element in the footprint pre-computing phase.

Finally, the blob-based method can produce significant savings in cases where the image to be projected consists of just a few or even a single non-zero element, such as in a recently proposed method for fast estimation of resolution and covariance in SPECT [7].

ACKNOWLEDGEMENTS

The authors gratefully acknowledge Dr. Kenneth F. Koral for ongoing discussions and collaboration. This work was supported by NCI grants R01 CA-87955 and CA-60711 and NSF grant BES-9982349.

REFERENCES

[1] E. V. R. Di Bella, A. B. Barclay, R. L. Eisner, and R. W. Schafer, "Comparison of rotation-based methods for iterative reconstruction algorithms," in *Proc. IEEE Nuc. Sci. Symp. Med. Im. Conf.*, vol. 2, 1995, pp. 1146–50.

[2] S. Matej and R. M. Lewitt, "Practical considerations for 3-D image reconstruction using spherically symmetric volume elements," *IEEE Tr. Med. Im.*, vol. 15, no. 1, pp. 68–78, Feb. 1996.

[3] G. L. Zeng and G. T. Gullberg, "Unmatched projector/backprojector pairs in an iterative reconstruction algorithm," *IEEE Tr. Med. Im.*, vol. 19, no. 5, pp. 548–55, May 2000.

[4] M. Unser, P. Thevenaz, and L. Yaroslavsky, "Convolution-based interpolation for fast, high quality rotation of images," *IEEE Tr. Im. Proc.*, vol. 4, no. 10, pp. 1371–81, Oct. 1995.

[5] R. M. Lewitt, "Multidimensional digital image representations using generalized Kaiser-Bessel window functions," *J. Opt. Soc. Am. A*, vol. 7, no. 10, pp. 1834–46, Oct. 1990.

[6] ——, "Alternatives to voxels for image representation in iterative reconstruction algorithms," *Phys. Med. Biol.*, vol. 37, no. 3, pp. 705–16, Mar. 1992.

[7] J. W. Stayman and J. A. Fessler, "Fast methods for approximation of resolution and covariance for SPECT," in *Proc. IEEE Nuc. Sci. Symp. Med. Im. Conf.*, 2002, to appear.